lubricants

MDPI

Article

An Investigation on the High-Temperature Stability and Tribological Properties of Impregnated Graphite

Juying Zhao [1], Qi Xin [2], Yunshuang Pang [2], Xiao Ning [2], Lingcheng Kong [2], Guangyang Hu [2], Ying Liu [1], Haosheng Chen [1] and Yongjian Li [1,*]

[1] State Key Laboratory of Tribology in Advanced Equipment, Tsinghua University, Beijing 100084, China; zhaojuyi18@mails.tsinghua.edu.cn (J.Z.)
[2] Shenyang Engine Research Institute, Aero Engine Corporation of China, Shenyang 110015, China
* Correspondence: liyongjian@tsinghua.edu.cn

Abstract: Impregnated graphite is a common material for friction pairs in aeroengine seals, especially at high temperatures. For the convenience of the application of graphite materials in aeroengines, an SRV-4 tribometer and a synchronous thermal analyzer are employed to study the tribological properties and thermal stability of pure, resin-impregnated, metal-impregnated, and phosphate-impregnated graphite against stainless steel from room temperature to 500 °C. The results indicate that impregnations can improve the wear resistance and thermal stability of graphite at high temperatures. Compared with other impregnated graphite materials, the resin-impregnated graphite shows a good friction coefficient and poor wear rate and thermal stability over 300 °C, due to the degradation and oxidation of the resin-and-graphite matrix. The metal- and phosphate-impregnated graphite materials exhibit excellent wear resistance and thermal stability under 500 °C as a result of the protection of the impregnations, while the average friction coefficient of the metal-impregnated graphite is much greater than the phosphate-impregnated graphite, and even reaches 2.14-fold at 300 °C. The wear rates for the graphite impregnated with resin, metal, and phosphate are 235×10^{-7}, 7×10^{-7}, and 16×10^{-7} $mm^3N^{-1}m^{-1}$ at 500 °C, respectively. Considering all aspects, the phosphate-impregnated graphite exhibits excellent tribological properties and thermal stability.

Keywords: graphite; high temperature; stability; wear mechanism

check for updates

Citation: Zhao, J.; Xin, Q.; Pang, Y.; Ning, X.; Kong, L.; Hu, G.; Liu, Y.; Chen, H.; Li, Y. An Investigation on the High-Temperature Stability and Tribological Properties of Impregnated Graphite. *Lubricants* **2024**, *12*, 388. https://doi.org/10.3390/lubricants12110388

Received: 9 October 2024
Revised: 28 October 2024
Accepted: 5 November 2024
Published: 13 November 2024

Copyright: © 2024 by the authors. Licensee MDPI, Basel, Switzerland. This article is an open access article distributed under the terms and conditions of the Creative Commons Attribution (CC BY) license (https://creativecommons.org/licenses/by/4.0/).

1. Introduction

The seal is a key component of an aeroengine bearing chamber, which plays an important role in preventing harmful leakage of the internal medium from the engine [1,2]. Because of the more severe working conditions and requirements of environmental protection, seals of engine bearing chambers need to have excellent performance under more challenging working conditions, such as higher pressure, higher speed, and higher temperature. At present, these are mostly contact seals, including mechanical seals, circumferential seals, split ring seals, and so on [3–6]. In the process of seal operation, intense friction occurs and may cause severe damage to the seal materials, resulting in the deformation of the seal surface and further deterioration of seal performance [7,8]. Therefore, it is of great significance to investigate the mechanisms of the friction and wear of common seal materials under harsh working conditions for the design and usage of engine seals.

Because of its excellent chemical stability, corrosion resistance, and tribological properties, graphite is widely used and investigated as a common seal material. Many materials can be paired with graphite material, such as stainless steel, ceramics, hard alloys, and so on [9–15]. Graphite has a layered crystal structure and a weak van der Waals force [16,17]. Thus, in the process of friction, wear debris can appear on the surface of graphite and then be transferred to the surface of the paired friction material [18,19]. At this moment, a transfer layer is formed, which further improves the tribological properties. However,

there are many pores in pure graphite materials sintered by hot pressing. Therefore, pure graphite materials have poor strength and wear resistance. Graphite materials oxidize easily at high temperatures, leading to a further decline in material properties. These factors limit the range of application and service life of graphite as a seal friction pair material under high-temperature conditions. In order to improve the performance and further expand the usage of graphite materials, two methods are commonly used. One method is to form a composite material with graphite powder and other materials [20–22], and the other is to impregnate the graphite sintered by hot pressing [23–25]. Compared with the former, impregnated graphite can maintain more tribological properties of pure graphite, as this kind of graphite is evolved from the whole matrix of graphite.

When the pores of graphite are filled with resin, metal, phosphates, and other components, the oxidation resistance and tribological properties of graphite materials are enhanced [26–28]. Much attention has been paid to the tribological properties of impregnated graphite at room temperature (R.T.). And there are also a small number of studies concentrating on the tribological characteristics of graphite materials impregnated with resin and phosphates at temperatures under 350 °C [28–31]. Zhao et al. conducted a friction study on graphite material impregnated with resin using the ball-against-disk test, and found that the surface of impregnated graphite material at 160 °C can maintain stability. It showed better high-temperature tribological performance compared with pure graphite [29]. The impregnation of phosphate materials can induce the appearance of a unique double taper on the surface of the flat friction pair, which is caused by the breakage, transference, accumulation, and abrasion of the impregnated components in graphite at 80 °C [32]. In conclusion, impregnated components have a complex and comprehensive influence on the properties of graphite materials. Furthermore, graphite material is usually employed at more crucial temperatures over 350 °C in the field of aeroengine bearing chamber seals. Meanwhile, at extremely high temperatures, aeroengine seals can suffer significantly deteriorated working environments. The stability of graphite's friction and wear properties plays an important role in the performance and lifespan of the seal. The thermal stability of graphite materials, specifically the evolution of impregnations at high temperatures and their protective effects on the graphite matrix, is one of the crucial factors affecting the tribological properties of impregnated graphite. Moreover, the fragmentation and accumulation of impregnations in friction conditions are other significant factors influencing the tribological behavior of graphite under high temperatures. However, there have been few studies on the comparison of the friction and wear mechanisms of different kinds of impregnated graphite at high temperatures. Furthermore, even fewer have concentrated on the relationship between high-temperature thermal stability and the tribological properties of impregnated graphite. These fields possess considerable potential for further investigation.

In this study, pure graphite and three widely used graphite materials impregnated with resin, metal, and phosphates were selected to carry out friction and wear tests with stainless steel friction pairs under different temperature conditions (R.T., 100 °C, 300 °C and 500 °C). The mechanisms of high-temperature stability and tribological properties of different impregnated graphite materials were revealed by means of scanning electron microscopy, thermogravimetric analysis, and other methods. Thermal stability is not only a characterization of graphite materials but also a helpful metric by which to analyze the mechanisms of tribological properties at high temperatures. This study can be helpful for research on impregnated graphite materials and the application of graphite materials in aeroengines.

2. Materials and Methodology

2.1. Materials

The pure, resin-impregnated, and metal-impregnated graphite were provided by Folken Co., Ltd. (Ningbo, Zhejiang, China), with open porosities of less than 15%, 3%, and 3%, respectively. The phosphate-impregnated graphite material, purchased from Morgan

New Material Co., Ltd. (Shanghai, China), had an open porosity of less than 7%. The basic properties of the four kinds of graphite materials, including the compressive strength, density, open porosity and so on, are clarified in Table 1. The friction pair material against graphite was stainless steel. In this study, the graphite material was manufactured into a disk with a diameter of 24 mm. The shape of the stainless steel disk was slightly complex. The lower half of the stainless steel disk was an 11 mm cylinder, used as the friction pair against the graphite disk in the test. And the upper half of the stainless disk was a 23 mm cylinder with a conical hole in the center to be loaded and driven during the test. The roughness of the graphite and stainless steel disks was designed to be no more than 0.2 μm and 0.1 μm, respectively. More details of the stainless steel and the graphite disks can be found in Figure 1b,c in Section 2.2.

Table 1. Physical properties of pure graphite and impregnated graphite.

Material	Compressive Strength (≥MPa)	Flexural Strength (≥MPa)	Density (≥g/cm^3)	Open Porosity (≤%)	Coefficient of Thermal Expansion (1/K)
Pure graphite	85	30	1.56	15.0	4.0×10^{-6}
Resin-impregnated graphite	182	55	1.62	2.0	4.5×10^{-6}
Metal-impregnated graphite	170	55	2.2	3.0	5.0×10^{-6}
Phosphate-impregnated graphite	98	44	1.8	7.0	7.0×10^{-6}

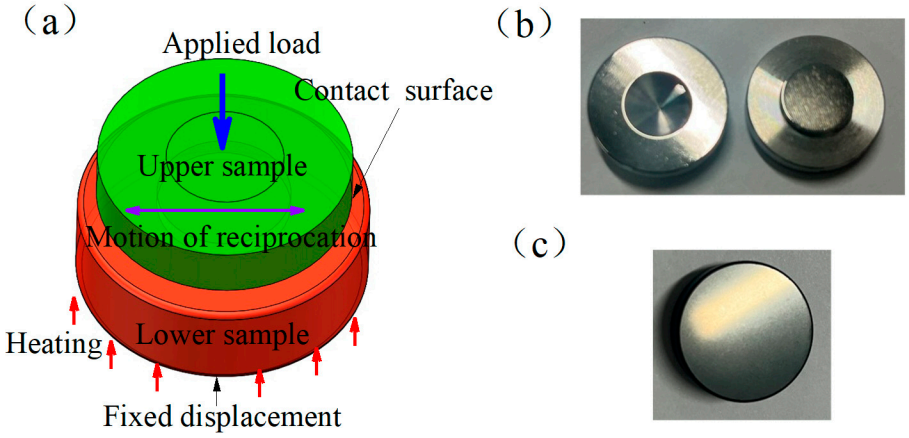


Figure 1. Schematic diagram of friction test and test samples: (**a**) friction test and sliding directions; (**b**) stainless steel sample (left side—top view; right side—bottom view); (**c**) graphite sample.

2.2. Friction Test

The high-temperature friction and wear tests of the graphite materials were carried out in a disk-on-disk manner using a high-temperature tribotester (SRV-4, Optimol, Munich, Germany) under dry friction conditions. The SRV-4 is a commonly used high-temperature tribometer with the advantages of high operating temperature and fixtures capable of meeting the requirements of different friction pairs, for instance, the disk-on-disk pattern in this study. The relative motion mode of the test samples is shown in Figure 1a. The upper and lower samples were graphite and stainless steel disks, as shown in Figure 1b,c. During the friction tests, the graphite disk was first fixed on the worktable of the SRV-4, and then, the stainless steel disk was mounted on the drive shaft of the SRV-4 through the conical hole. The SRV-4 machine was adjusted to ensure full contact of the friction surface between the graphite and the stainless steel disks. Then, the temperatures of the experimental cavity were heated to the preset values (R.T., 100 °C, 300 °C, and 500 °C). When the temperature was stable, the corresponding friction test could be carried out. In the tests, the reciprocating frequency was 50 Hz, while the applied load was 50 N, and

these conditions are typical for an aeroengine seal. The friction test duration of each group was 1800 s. The SRV-4 was equipped with a sensor to record the friction force and load in the process of the friction test, and these data were transmitted to a nearby computer for the calculation of the corresponding friction coefficient. After the tests, the friction pairs were taken out and cleaned with alcohol in an ultrasonic cleaner for 10 min.

2.3. Measurement and Characterization

The wear rate is an important parameter to evaluate the performance of different graphite materials at high temperature. In this paper, the wear rates were obtained by measuring the wear mass loss. The wear rate (ω) of graphite materials at high temperatures can be calculated using Equation (1), where m_0 and m_1 are the masses of the graphite sample before and after the friction test, respectively; N is the number of reciprocating motion periods of the stainless steel sample; d is the distance of the reciprocating motion period, which is 1 mm in the test; ρ is the density of the corresponding graphite material; and F is the positive force added in the test.

$$\omega = \frac{m_0 - m_1}{\rho N d F} \quad (1)$$

Many test methods were adopted to reveal the friction and wear mechanisms of different kinds of graphite materials at different temperatures. Before and after the friction tests, white light interferometry (New View 8300, Zygo, CT, USA) was used to observe and measure the surface roughness and wear marks of different graphite materials. The friction and wear characteristics of graphite materials at high temperatures are closely related to their thermal stability. Furthermore, in order to characterize the high-temperature stability of the four graphite materials, the graphite was heated to 500 °C and held in an air atmosphere for 5 h in a high-temperature chamber, and the oxidation of graphite was observed. The weight loss percentages were calculated according to the weight results of graphite materials before and after the high-temperature oxidation. To investigate the mechanisms of weight loss at high temperatures, thermogravimetric analyses of the graphite materials were further carried out using an NETZSCH STA 449F3 synchronous thermal analyzer (NETZSCH, Hanau, Germany) in an air atmosphere, where the temperatures ranged from R.T. to 600 °C and the heating rate was 10 °C/min. The released gasses of the corresponding graphite materials from the synchronous thermal analyzer were further investigated through Fourier infrared spectroscopy (FTIR, Bruker VERTEX70v, Saarbrucken, Germany). The hardness of the different graphite materials at R.T. and high temperatures was measured by a high-temperature hardness tester (Zongde, Qingdao, China). In addition, scanning electron microscopy (SEM, Quanta 200, FEI, Billings, MT, USA) was used to observe the morphology, and energy-dispersive X-ray spectroscopy (EDS, EDS, Genesis xm-2, EDAX, Pleasanton, CA, USA) was used to analyze the distribution of elements on the graphite surface before and after the friction tests.

3. Results and Discussion

3.1. Friction and Wear Behavior

The coefficient of friction is a pivotal physical parameter that delineates the tribological characteristics of materials. Under a load of 50 N and a frequency of 50 Hz, the average friction coefficient for four graphite materials varies with increasing temperatures, as illustrated in Figure 2a. For the pure graphite, the friction coefficients remain relatively constant at R.T. and 100 °C, and have a noticeable decline at 300 °C. Considering the strength of material and the safety of the experiment, the friction and wear tests were not conducted for the pure graphite at 500 °C. For the resin-impregnated graphite, the friction coefficients show a decreasing trend with an increase in temperatures, gradually reducing from 0.278 at R.T. to 0.179 at 500 °C. The reduction in the friction coefficients may be related to the phase transition of the resin-impregnated graphite and the formation of a graphite transfer layer at the friction interface. For the metal-impregnated graphite, it can

be observed from Figure 2a that the average friction coefficients first increase significantly and then decrease with a rise in temperatures, reaching a peak value of 0.536 at 300 °C. Under the same temperature conditions, the friction coefficients of the metal-impregnated graphite are higher than that of the resin-impregnated graphite, which differs from the findings in the literature [27,30]. This discrepancy may be due to the differences in the test conditions (contacting pattern, surface roughness, testing environments, and so on). For the phosphate-impregnated graphite at R.T., 100 °C, 300 °C, and 500 °C, the corresponding friction coefficients are 0.291, 0.251, 0.251, and 0.278, respectively. These results indicate that temperature variations have a slight effect on the average friction coefficients of the phosphate-impregnated graphite.

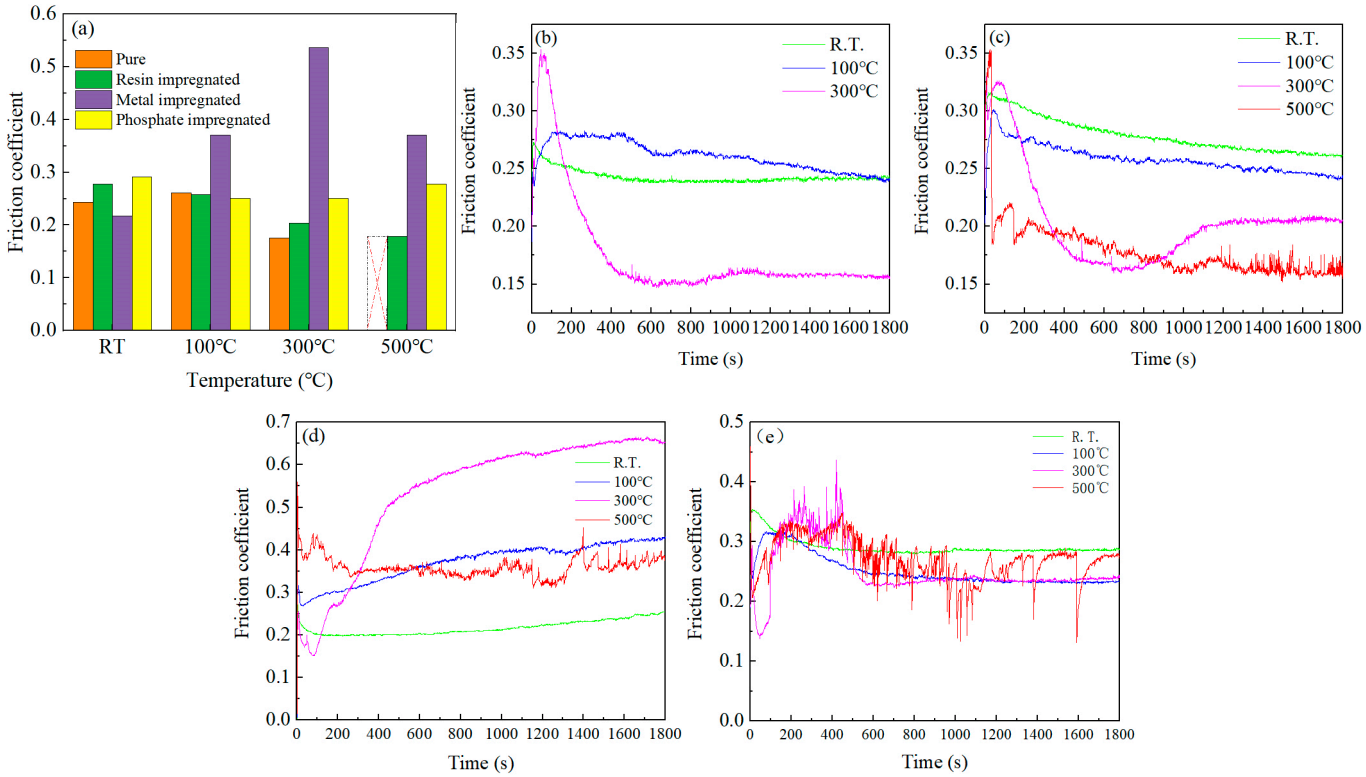


Figure 2. Friction coefficients of graphite materials under different working conditions. (**a**) Average friction coefficient; (**b**) pure graphite; (**c**) resin-impregnated graphite; (**d**) metal-impregnated graphite; (**e**) phosphate-impregnated graphite.

Figure 2b to Figure 2e, respectively, show the changes in the friction coefficients of four graphite materials with test time at different temperatures. For the pure graphite materials and resin–graphite, the friction coefficients are relatively stable or have a slight decreasing trend with an increase in test time at R.T. and 100 °C. A significant decline in the friction coefficient is observed during the early part of the test at 300 °C, and then the friction coefficient has a minor increase and keeps stable. As can be seen from Figure 2d, for the metal-impregnated graphite materials, the friction coefficients increase with the test time at R.T., 100 °C, and especially 300 °C. For the graphite material impregnated with phosphate, the friction coefficients remain stable after the initial running-in stage at no more than 300 °C. At 500 °C, the friction coefficients of these three impregnated graphite materials fluctuate sharply.

Under different temperature conditions, the wear rates of four graphite materials calculated according to Equation (1) are shown in Figure 3. The wear rates of all kinds of graphite materials are small at R.T., no more than 2.0×10^{-7} $mm^3N^{-1}m^{-1}$. The wear rates of the pure graphite material and phosphate-impregnated graphite material are slightly higher than those of the resin-impregnated and metal-impregnated graphite materials. This

may be due to the lower hardness of the graphite material impregnated with phosphates compared to the other two impregnated graphite materials, as clarified in Section 3.2. The pure graphite materials have terrible performance in terms of their wear rates with an increase in temperature. At 100 °C and 300 °C, the wear rate of the pure graphite materials is the largest one among the tested graphite samples, because there is no protection of the impregnation components. For the resin-impregnated graphite materials, the wear rates increase rapidly with a rise in temperature. The resin-impregnated graphite exhibits wear rates that are 3.6-fold and 14.0-fold higher than the maximum wear rate observed for the metal-and phosphate-impregnated graphite materials, at 300 °C and 500 °C, respectively. This phenomenon may be due to the damage to the resin–graphite material caused by the high temperature. For the metal-impregnated and phosphate-impregnated graphite materials, it can be found that the wear rates of both kinds of graphite increase moderately with temperature, due to the high stability at high temperatures. These results will be further clarified in Section 3.2. In addition, in different temperature conditions, the wear rates of the metal-impregnated graphite material are smaller than those of the phosphate-impregnated graphite material.

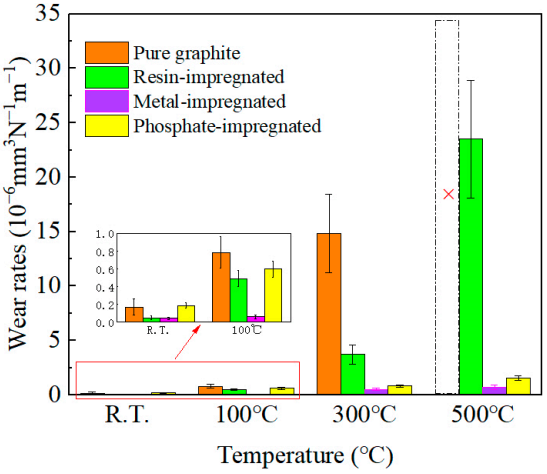


Figure 3. The wear rates of the four graphite materials at different temperatures. ("×" indicates that the group did not undergo a friction test for safety reasons).

Figure 4 shows the surface morphology, measured using white light interferometry, of different graphite materials under various temperatures conditions. It can be observed that the surface roughness of the graphite materials before the wear test is relatively low, and the surfaces are quite smooth. The roughness values for the four types of clean graphite materials range from 0.033 μm to 0.048 μm. For the pure and the resin-impregnated graphite materials, the surface roughness does not show significant differences compared to the clean samples, and no obvious wear marks are observed on the surfaces of graphite at R.T. However, the surface roughness of the resin-impregnated graphite increases with temperature and reaches 1.330 μm at 500 °C. It can be observed that furrow wear appears on the surface of the resin-impregnated graphite. For the metal-impregnated graphite materials, abrasive wear plays an important role in the wear mechanisms at R.T. and 100 °C, with evidence of noticeable furrow wear on the friction surface. As the temperature increases, the furrow wear becomes unapparent, and meanwhile, the surface roughness decreases, which may indicate a change in the wear mechanisms. There is clear furrow wear on the surface of the phosphate-impregnated graphite materials, ranging from R.T. to 500 °C, and it can be inferred that abrasive wear is the main wear mechanism. Under high-temperature conditions, the tribological performances of the four types of graphite materials exhibit significant differences, which are attributed to the distinct components impregnated within the graphite matrices. Subsequent sections of this paper delve into

the thermal and mechanical properties of the graphite materials under high-temperature conditions, aiming to elucidate the disparities in their wear performance.

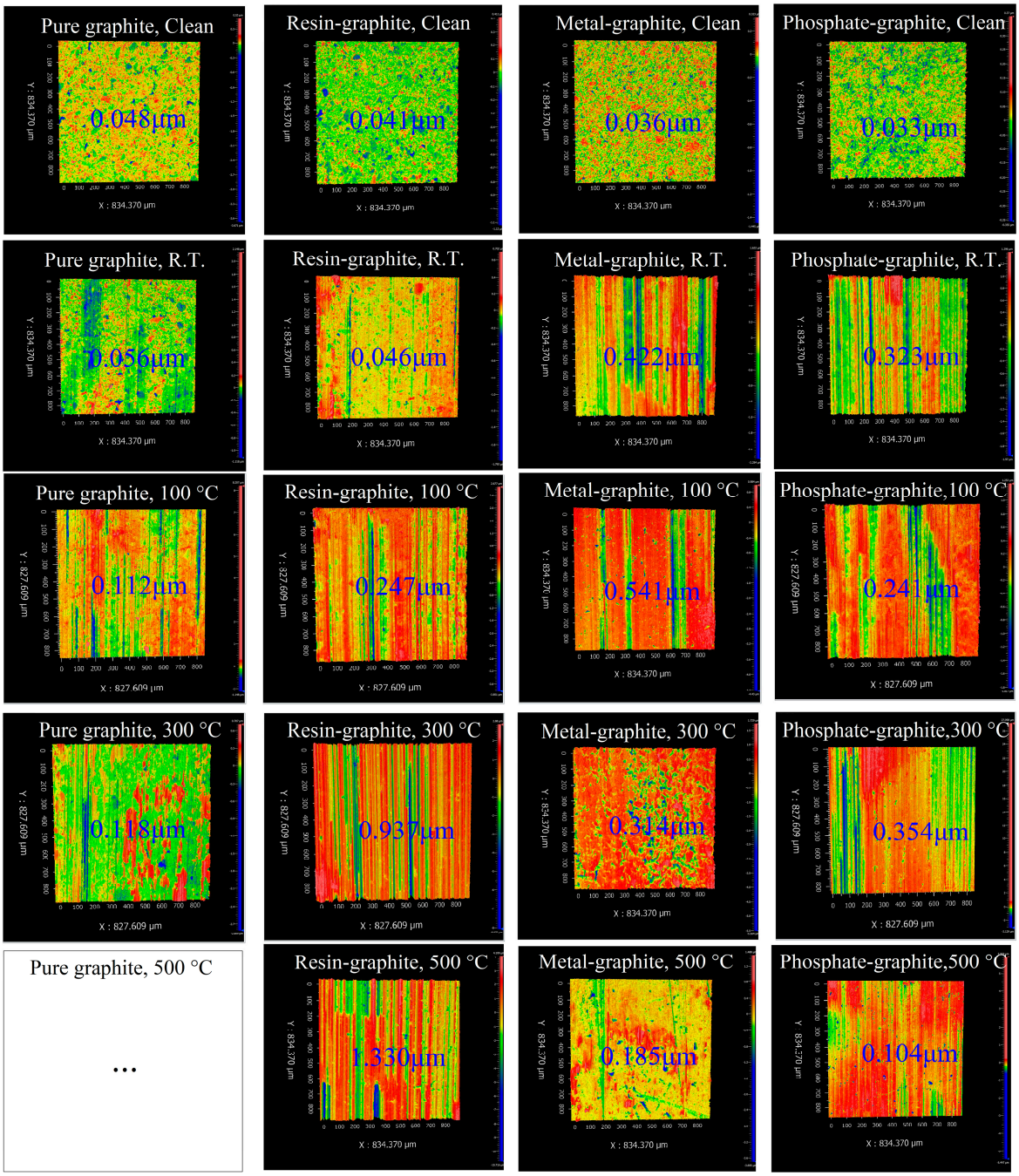


Figure 4. Surface morphologies of four graphite materials under different working conditions. (The ellipsis indicates that the group has not undergone a friction test for safety reasons).

3.2. Analysis of Thermal and Mechanical Properties of Materials

To further analyze the tribological performance and thermal stability of the graphite materials impregnated with different components under high-temperature conditions, prolonged heating tests, synchronous thermal analysis, and hardness tests were conducted on various types of graphite materials. These tests aimed to demonstrate the friction and wear mechanisms of the different impregnated graphite materials under high temperatures.

The graphite materials were supposed to work stably for a long period in the application of the seal devices. The prolonged heating tests were carried out for the four types of

graphite materials, which were placed in an air atmosphere for 5 h at 500 °C. As shown in Figure 5, the mass loss rates after heating were 21.58%, 9.83%, 0.07%, and 0.08% for the pure, the resin-impregnated, the metal-impregnated, and the phosphate-impregnated graphite, respectively. Many carbon powders were observed off the pure graphite sample, which underwent a destructive change in long-term high-temperature oxidative environments. The resin-impregnated graphite performed better than the pure graphite, while the metal-impregnated and phosphate-impregnated graphite materials showed minimal changes. In conclusion, the oxidation resistance of the four graphite materials under high-temperature conditions can be ranked as metal-impregnated ≈ phosphate-impregnated ≫ resin-impregnated > pure graphite.

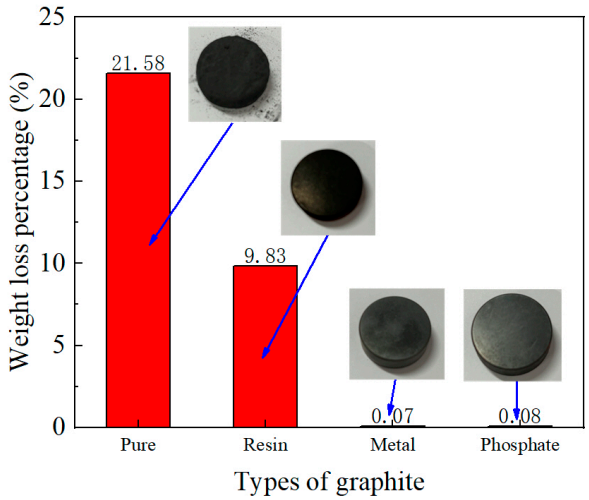


Figure 5. Mass loss rates of different graphite materials after 5 h prolonged heating tests. (The blue arrow indicates the correlation between the weight loss percentage of the graphite and the images of the graphite samples after the tests).

To investigate the mass loss mechanisms of the four graphite materials in the heating tests, Thermogravimetric Fourier Transform Infrared Spectroscopy (TG-FTIR) analysis was performed on the graphite samples in an oxidative atmosphere. Figure 6a illustrates the change in the graphite mass as the ambient temperature is increased from R.T. to 600 °C at a heating rate of 10 °C/min. It is observed that the pure graphite material loses mass at first, with the most pronounced mass loss (nearly 9%) at 600 °C among the four graphite materials. The resin-impregnated graphite remains nearly stable below about 250 °C, while the mass loss per minute increases rapidly at a temperature over 250 °C. And then, the mass loss of the resin-impregnated graphite reaches a value comparable to that of the pure graphite at 600 °C, which indicates a complete failure of the resin's protective effect. The masses of the metal-and phosphate-impregnated graphite materials remain almost stable under about 550 °C and show a slight decrease in the range of 550 °C to 600 °C, which supports the application of these two graphite materials under high temperatures.

The differential scanning calorimetry (DSC) curve represents the thermal effects caused by the physical and chemical transformations of the tested materials during heating, aiding in the analysis of the thermal behaviors. As shown in Figure 6b, the pure graphite material exhibits an exothermic reaction from the initial temperature. This reaction intensifies with an increase in temperatures in the range of R.T. to 600 °C, which indicates an acceleration in the oxidation of the pure graphite. The resin-impregnated graphite material shows an endothermic reaction at first, which may be attributed to the oxidation resistance of the resin components. The characteristics of the exothermic reaction occur over about 250 °C, implying a decrease in the resin's protection. When the heating temperatures exceed about 540 °C, the exothermic effect of the graphite further intensifies and approaches that of the pure graphite, indicating the failure of the resin's protective effect. The protection effects

of the impregnated components may be caused by the phase transition and the oxidation of the resin materials itself. For the metal-and phosphate-impregnated graphite materials, the trends of the DSC curves remain relatively stable, with positions below the zero axis for nearly all testing temperatures. There is a slight increase when the temperatures reach around 540 °C, which is due to the diminishing protective effect of the metal and phosphate.

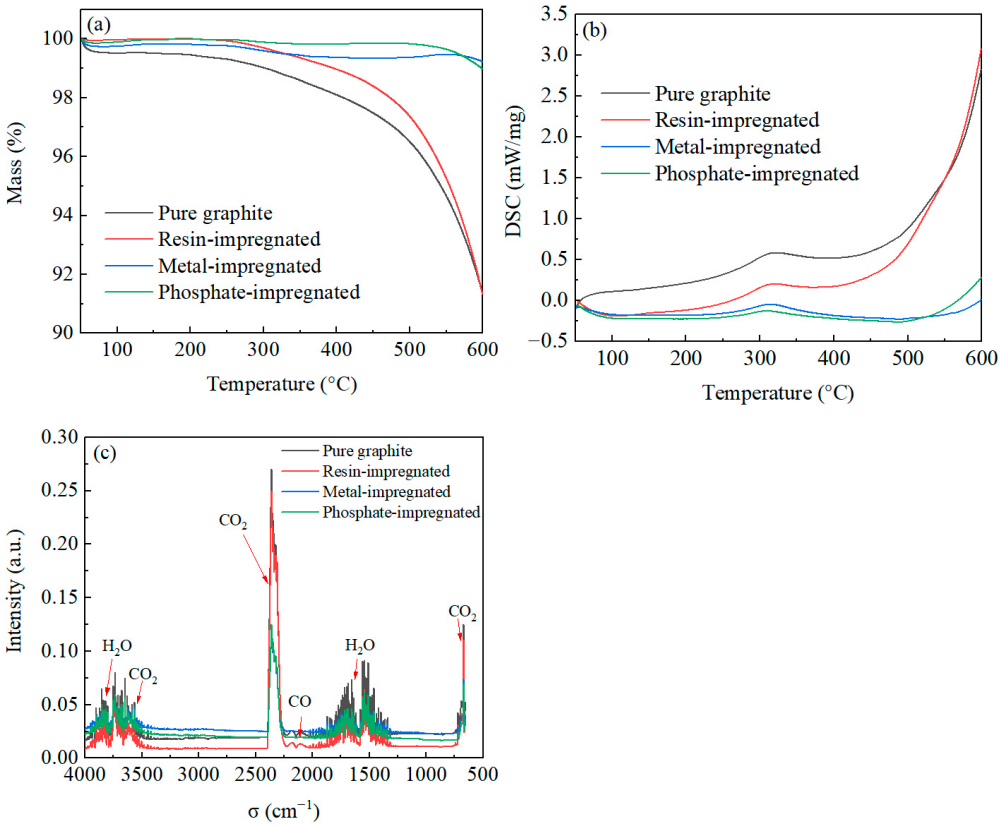


Figure 6. Test results of thermal stability for different graphite materials. (**a**) Thermogravimetric curves, (**b**) DSC curves, (**c**) FTIR curves.

The gasses emitted from the TG instrument were simultaneously analyzed using the FTIR method. The instrument records the infrared spectra at different temperatures, and the obtained spectra (absorbance vs. wavenumber) can be compared and analyzed against the gas-phase infrared spectral library. In situ FTIR spectra collection aids in the qualitative analysis of the changes in the evolved graphite materials. The spectra corresponding to 500 °C for the four types of graphite materials are shown in Figure 6c. According to previous studies, the intensity peaks in the ranges of 4000–3500 cm^{-1} and 2000–1300 cm^{-1} correspond to the O-H bonds, implying the existence of H_2O [33,34]. The intensity peaks in the range of 3760–3500 cm^{-1}, 2400–2220 cm^{-1}, and 680–650 cm^{-1} correspond to the C = O bonds, indicating the presence of CO_2 [33,35]. Additionally, the intensity peaks in the range of 2000–2250 cm^{-1} correspond to the C≡O bonds, suggesting the existence of CO [35]. The functional groups identified in the literature are used to annotate Figure 6c. It is found that all four types of graphite materials produce CO_2 and H_2O. Due to the overlap in the CO_2 peaks in the range of 3760–3500 cm^{-1} with the broad peaks of H_2O spanning from 4000 to 3500 cm^{-1}, the alternative characteristic peaks are utilized to assess the enrichment levels of CO_2 [35,36]. The pure graphite and resin-impregnated graphite exhibit stronger CO_2 peaks and minor CO peaks, indicating significant oxidation of the graphite materials. In contrast, the metal-and phosphate-impregnated graphite show weaker CO_2 peaks and no CO peaks, indicating better oxidation resistance of the graphite materials.

According to the analysis of the TG-FTIR results, we can draw conclusions regarding the degrees of oxidation resistance of the four types of graphite, which are in good agreement with the findings from the long-term thermal oxidation experiments, as shown in Figure 5.

To further evaluate the overall performance of the impregnated graphite materials under high-temperature conditions, the hardness of the resin-impregnated, metal-impregnated, and phosphate-impregnated graphite materials was measured at R.T. and 500 °C. The results are shown in Figure 7. To elucidate the hardness results more clearly, the normalized hardness is defined as the ratio of the measured hardness of the graphite material and the maximum of all measured hardness data. It can be observed that the hardness of both the resin- and phosphate-impregnated graphite materials decreased at 500 °C compared with R.T., while the hardness of the metal-impregnated graphite increased in the same situation. This phenomenon will be clarified in Section 3.3, referring to the SEM results.

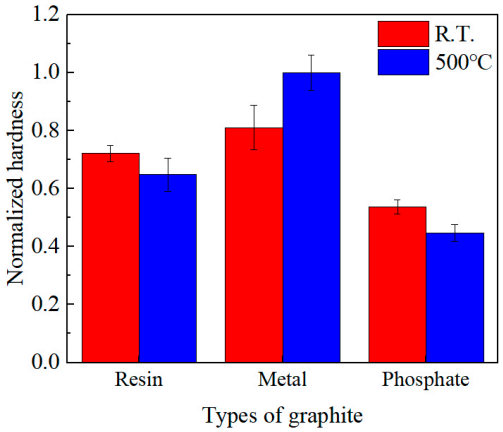


Figure 7. Normalized hardness of different graphite materials under high temperature.

3.3. Wear Mechanisms Analysis of Graphite Materials

The SEM results can further provide insights into the friction and wear mechanisms occurring on the graphite surface. The SEM images were obtained for the different graphite materials after friction tests at R.T. and 500 °C. The clean and worn images were taken from the unworn and worn areas of the corresponding graphite materials after the friction tests, respectively. Additionally, the EDS analysis was performed on the metal-impregnated graphite material.

Figure 8a,b show the SEM images of the pure graphite before and after the friction tests at R.T. The dark areas are carbon, which occupy the majority of the image. The little spots are the aggregation of small amounts of impurities. It can be observed that the surface of the worn pure graphite is relatively smooth with a few wear scars. Under high-temperature conditions, prolonged oxidation can lead to significant structural degradation in the pure graphite, rendering the surface of the graphite less dense and more friable. This deterioration makes it challenging to perform friction and SEM tests for the pure material. Thus, the observations were limited to the wear results at R.T. for the graphite material. Figure 8c–g present the SEM images of the resin-impregnated graphite before and after the friction tests at R.T. and 500 °C. After the friction test at R.T., the surface of the resin-impregnated graphite remains relatively smooth with only a few wear scars. After oxidation in high-temperature environments, the surface of the resin-impregnated graphite at 500 °C is as shown in Figure 8e. It can be observed that there are some pore defects on the surface of the graphite materials. It can be inferred from Figure 6 that the thermal stability of the resin-impregnated graphite deteriorates and the resin undergoes decomposition at 500 °C. This phenomenon leads to the formation of these pore defects, which further accelerate the oxidative degradation and reduces the wear resistance of the

graphite matrices. During the test, a large amount of obvious furrow wear appear on the friction areas of the resin-impregnated graphite. Further magnified observation reveals that chunks of the resin and graphite have detached from the worn areas of the material. The degradation of the resin decreases the strength of the graphite regions that were previously filled with the impregnations, making the graphite more prone to fragmentation. These fragments become the abrasive particles that enter the friction interface, thereby exacerbating the wear on the graphite surface.

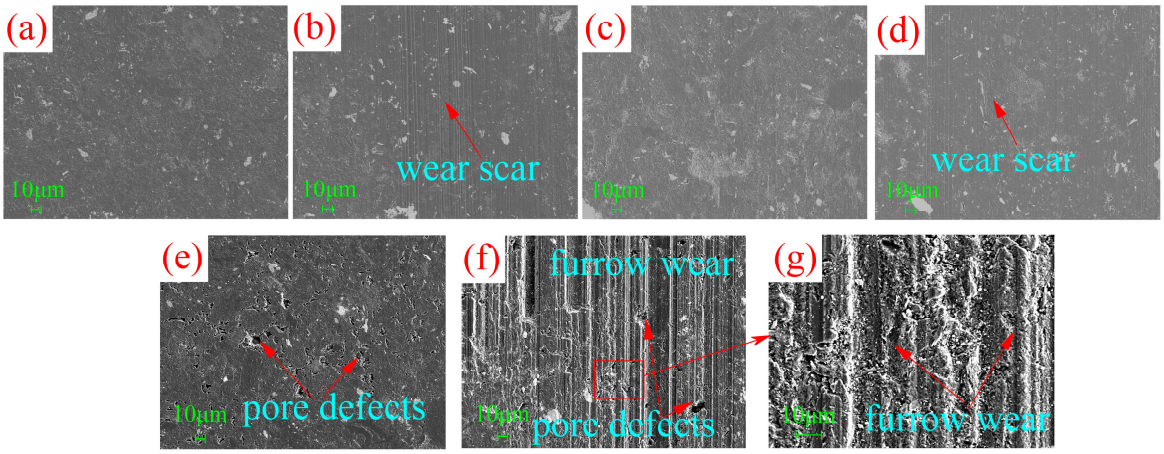


Figure 8. The SEM results of the pure graphite and resin-impregnated graphite at R.T. and 500 °C: (**a**) clean pure graphite at R.T., (**b**) worn pure graphite at R.T., (**c**) clean resin–graphite at R.T., (**d**) worn resin–graphite at R.T., (**e**) clean resin–graphite at 500 °C, (**f**) worn resin–graphite at 500 °C (400×), (**g**) worn resin–graphite at 500 °C (1000×).

For the metal-impregnated graphite materials, the metal phases are distributed as clumps or even network structures in the graphite matrices before friction tests, as shown in Figure 9a. During the test, the surface of the metal-impregnated graphite undergoes friction, and exhibits furrow wear at R.T. (Figure 9b,c), which is consistent with the measured results of the white light interferometry. At 500 °C, the unworn areas of the graphite surface are as shown in Figure 9d. It can be observed that the oxidation of the graphite matrix results in the formation of some pore defects. The metal phase has been oxidized to form antimony oxides, yet the network structures are retained, which increases the hardness of the metal-impregnated graphite at 500 °C compared with R.T. Meanwhile, although several parts of the surface layer of the graphite matrices are oxidized and some pore defects are formed at 500 °C, the oxidation of antimony metal itself and the formation of the antimony network prevent further oxidation of the graphite matrices, protecting the deeper layer of graphite matrices, and enhancing the high-temperature stability and wear resistance of the metal-impregnated graphite. These further corroborate the results shown in Figures 6 and 3, respectively. During the friction test, the friction mechanisms changed, and no distinguished furrow wear was observed, and simultaneously a wear layer of the antimony oxides was formed on the surface of the graphite material, as shown in Figure 9e,f, which may decrease the roughness of the graphite surface. Meanwhile, this wear layer may further reduce the wear rates of the metal-impregnated graphite compared with other impregnated graphite materials.

The elemental contents and distributions on the surface of the metal-impregnated graphite were analyzed using the EDS method. The comparative atomic and mass contents of fundamental elements on the surface of the metal-impregnated graphite materials are illustrated in Table 2, for the clean graphite at R.T. and the worn graphite at 500 °C, respectively. The metal-impregnated graphite materials are mainly composed of carbon, antimony, oxygen, iron, and nickel (C, Sb, O, Fe and Ni), which constitute more than 99 percent of the total mass. Compared with the clean graphite at R.T., a discernible

reduction in the C content and a concurrent increase in the O content occurs after the friction test at 500 °C. This indicates that the high-temperature wear process leads to relative depletion of the carbon and an enrichment in the oxygen at the material's surface.

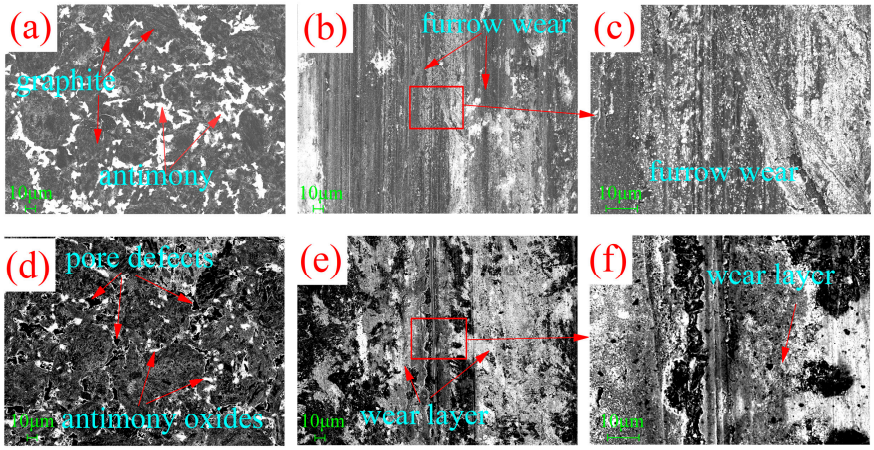


Figure 9. The SEM results of the metal-impregnated graphite at R.T. and 500 °C: (**a**) clean metal–graphite at R.T., (**b**) worn metal–graphite at R.T. (400×), (**c**) worn metal–graphite at R.T. (1000×), (**d**) clean metal–graphite at 500 °C, (**e**) worn metal–graphite at 500 °C (400×), (**f**) worn metal–graphite at 500 °C (1000×).

Table 2. Fundamental elemental contents of the impregnated metal–graphite materials.

	Clean Metal-Impregnated Graphite		Worn Metal-Impregnated Graphite	
	Mass Fraction	**Atomic Fraction**	**Mass Fraction**	**Atomic Fraction**
C	67.31%	92.46%	62.99%	87.35%
O	2.90%	2.99%	7.72%	8.03%
Sb	27.62%	3.74%	27.01%	3.69%
Fe	1.10%	0.32%	1.20%	0.36%
Ni	0.28%	0.08%	0.37%	0.10%

Figure 10 presents the EDS results of the clean metal-impregnated graphite material at R.T. In the EDS elemental distribution images, each element is represented by a distinct color, with the brighter areas indicating a higher concentration of the element at that location. It is observable that the carbon matrices and the main impregnated metal, Sb, exhibit a mutually exclusive distribution across the graphite surface. The oxygen is ubiquitously distributed across the surface of the graphite material, with relative enrichment observed in the regions containing the Sb element. After the wear test at 500 °C, a distinct wear layer forms on the metal-impregnated graphite surface, as shown in Figure 11. The C and Sb elements are both distributed within this wear layer, with a sparser pattern for C and a concentrated pattern for Sb. The reason for the sparser pattern of C is probably that the graphite matrices were worn during the friction tests and some C elements were mixed in the wear layer. The bright regions for O coincide with those for Sb in the wear layer, suggesting that Sb was oxidized and formed an oxide wear layer that protected the carbon matrices and mitigated the oxidation rates of the graphite. Thus, the excellent thermal stability and the formation of a hard wear layer together result in the smallest wear rates of the metal-impregnated graphite at 500 °C compared with other impregnated graphite, as shown in Figure 3.

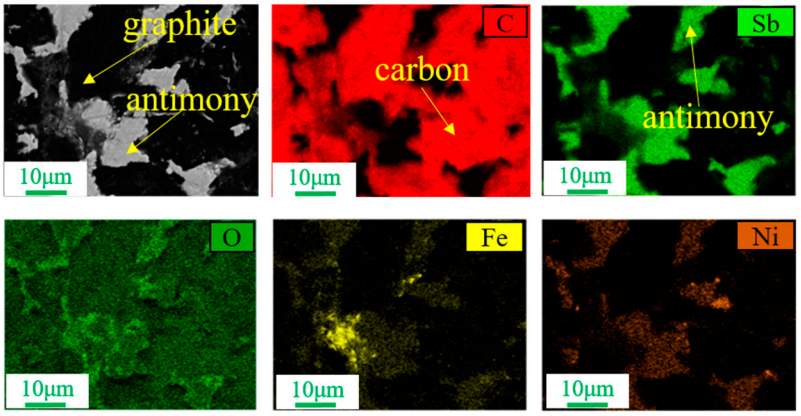


Figure 10. Energy spectrum distribution of the worn area of the metal-impregnated graphite at R.T.: C (red), Sb (light green), O (dark green), Fe (light yellow), Ni (orange).

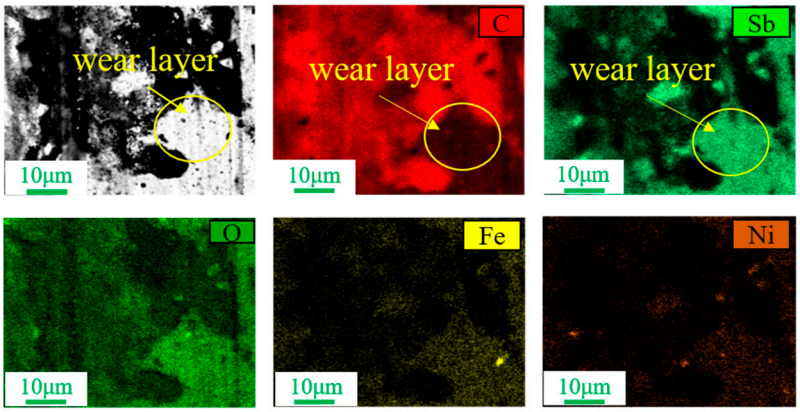


Figure 11. Element distribution of the unworn area of metal impregnated graphite materials at 500 °C: C (red), Sb (light green), O (dark green), Fe (light yellow), Ni (orange).

For the phosphate-impregnated graphite materials, phosphates are relatively uniformly distributed throughout the graphite matrices, as shown in Figure 12a. During the wear tests, the graphite sustains minor destruction at R.T., with most of the phosphates still embedded in the graphite matrices. The abrasion of the graphite material's surface is intensified by the detachment of the phosphates, with Figure 12b demonstrating that abrasive wear is the primary mode of graphite material loss. As shown in Figure 12c, the clean graphite surface maintains a relatively smooth state at 500 °C, with no apparent pores, which suggests that the graphite material impregnated with the phosphates exhibits superior oxidative resistance properties. Simultaneously, as corroborated by Figure 6, the graphite impregnated with phosphates exhibits outstanding thermal stability at 500 °C. As illustrated in Figure 12d, there are some aggregations of the phosphates and few pore defects in the wear areas. During the friction test at 500 °C, the surface of graphite material suffers wear and oxidation, leading to more phosphates being exposed. These phosphates may undergo fragmentation, detachment, and migration, accumulating in the wear regions [32]. To some extent, this accumulation can affect the stability of the friction coefficient, and even exacerbate wear during the test.

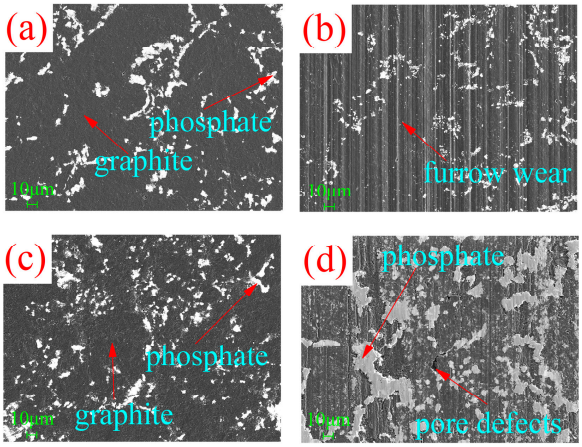


Figure 12. The SEM results of the phosphate-impregnated graphite at R.T. and 500 °C: (**a**) clean graphite at R.T., (**b**) worn graphite at R.T., (**c**) clean graphite at 500 °C, (**d**) worn graphite at 500 °C.

3.4. High-Temperature Stability and Tribological Properties of Graphite Materials

In order to provide guidance for the selection and application of graphite materials, it is essential to evaluate the stability of their tribological properties across a range of temperatures. These assessments are based on the friction and wear results, as well as the thermal stability of the graphite materials previously discussed. Figure 13 shows the comprehensive tribological properties of the graphite materials, including the tested friction coefficient and wear rates, under temperatures ranging from R.T. to 500 °C. The smaller the variations in the friction coefficient and wear rates, the better the stability of the tribological properties of the graphite materials. For both the pure graphite and the resin-impregnated graphite materials, the friction coefficients exhibit relatively good stability, while the stability of the wear rates is comparatively poor. In contrast, for the metal-impregnated graphite, the wear rate stability is relatively better, yet the stability of the friction coefficients is comparatively worse. In summary, the phosphate-impregnated graphite materials exhibit the most outstanding comprehensive performance under all temperatures conditions. In addition, for the convenience of the graphite material selection, a rating system was made to evaluate the materials comprehensively in terms of their friction coefficients, wear rates, and thermal stability, as shown in Table 3. The rating system utilizes a star-based approach, where a higher number of stars indicates more outstanding performance of the graphite material in the respective property.

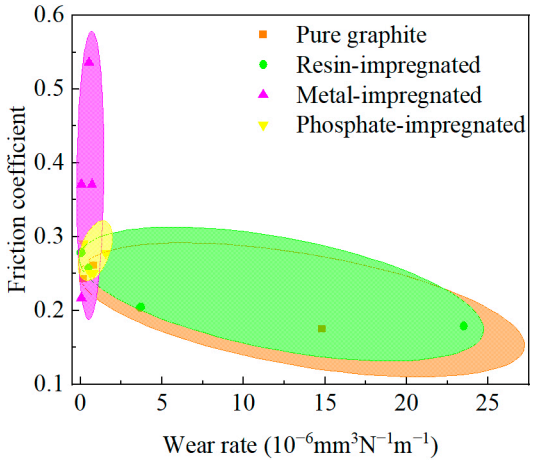


Figure 13. Tribological properties of graphite materials.

Table 3. Tribological properties of four graphite types.

Graphite Types	Friction Coefficient	Wear Rates	Thermal Stability
Pure	☆☆☆	☆	☆
Resin	☆☆☆☆	☆☆	☆☆
Metal	☆	☆☆☆☆☆	☆☆☆☆☆
Phosphate	☆☆☆☆☆	☆☆☆☆	☆☆☆☆☆

The more stars ("☆"), the better the performance of graphite in the respective property.

4. Conclusions

An experimental study was conducted on the tribological properties against stainless steel and thermal stability of four different graphite materials (pure, resin, metal, and phosphate) under high-temperature conditions. The analyses and discussions of the experimental phenomena lead to the following conclusions.

(1) As the test temperature increases, the friction coefficients of both the pure graphite and the resin-impregnated graphite materials remain relatively stable, while the wear rates increase rapidly and the thermal stability decreases. At elevated temperatures, the decomposition of the resin compromises the protective effect of the impregnated material on the graphite, resulting in degradation of the graphite's performance.

(2) The metal-impregnated graphite material exhibits excellent wear resistance and thermal stability at various test temperatures from R.T. to 500 °C. However, the friction coefficients significantly increase under the high-temperature conditions compared to R.T, with 0.217 at R.T. and 0.371 at 500 °C. Under high-temperature conditions, the metal is changed to form oxides. Concurrently, a wear layer is established during the friction process, which changes the tribological behavior of the graphite.

(3) With the elevation of temperatures, the average friction coefficients, wear rates, and thermal stability of the phosphate-impregnated graphite material remain comparatively stable, and this material exhibits the best tribological properties among the four tested graphite materials. Under high-temperature conditions, the wear rates increase, which may be attributed to the detachment, migration, and accumulation of the phosphate impregnations.

(4) At 500 °C, the thermal weight loss percentages for the graphite impregnated with resin, metal, and phosphate are 9.85%, 0.07%, and 0.08%, respectively, while the high temperature wear rates are 235×10^{-7} $mm^3N^{-1}m^{-1}$, 7×10^{-7} $mm^3N^{-1}m^{-1}$, and 16×10^{-7} $mm^3N^{-1}m^{-1}$, respectively. This indicates that the thermal stability at high temperatures has a crucial impact on the wear rates at high temperatures, and further, the properties of the impregnation itself, such as fragmentation and film formation, can affect the wear rates.

Author Contributions: J.Z.: investigation, writing—original draft. Q.X.: methodology, data curation. Y.P.: investigation, writing—original draft. X.N.: methodology. L.K.: investigation. G.H.: investigation, writing—review and editing. Y.L. (Ying Liu) and H.C.: methodology, funding acquisition. Y.L. (Yongjian Li): investigation, writing—review and editing. All authors have read and agreed to the published version of the manuscript.

Funding: Funding came from the National Science and Technology Major Project of China (2019-IV-0020-0088) and the National Science and Technology Major Project of China (2019-VII-0015-0155).

Institutional Review Board Statement: Not applicable.

Informed Consent Statement: Not applicable.

Data Availability Statement: The original contributions presented in this study are included in the article; further inquiries can be directed to the corresponding author.

Conflicts of Interest: Authors Qi Xin, Yunshuang Pang, Xiao Ning, Lingcheng Kong, Guangyang Hu were employed by the company Aero Engine Corporation of China. The remaining authors declare that the research was conducted in the absence of any commercial or financial relationships that could be construed as a potential conflict of interest.

References

1. Chupp, R.E.; Hendricks, R.C.; Lattime, S.B.; Steinetz, B.M. Sealing in turbomachinery. *J. Propul. Power* **2006**, *22*, 313–349. [CrossRef]
2. Michaelis, S. An update on aircraft oil bearing chamber sealing. *Seal. Technol.* **2018**, *2018*, 6–8. [CrossRef]
3. Mosavat, M.; Moradi, R.; Takami, M.R.; Gerdroodbary, M.B.; Ganji, D.D. Heat transfer study of mechanical face seal and fin by analytical method. *Eng. Sci. Technol. Int. J.* **2018**, *21*, 380–388. [CrossRef]
4. Nau, B.S. Mechanical seal face materials. *Proc. Inst. Mech. Eng. Part J J. Eng. Tribol.* **1997**, *211*, 165–183. [CrossRef]
5. Zhou, J.F.; Gu, B.Q.; Chen, Y. An improved design of spiral groove mechanical seal. *Chin. J. Chem. Eng.* **2007**, *15*, 499–506. [CrossRef]
6. Li, G.; Zhang, S.; Zhong, K.; Zhang, Y.; Zhu, J. Leakage and wear characteristics of carbon seals for aero-engines. *Chin. J. Aeronaut.* **2022**, *11*, 389–400. [CrossRef]
7. Hirani, H.; Goilkar, S. Formation of transfer layer and its effect on friction and wear of carbon–graphite face seal under dry, water and steam environments. *Wear* **2009**, *266*, 1141–1154. [CrossRef]
8. Ojile, J.O.; Teixeira, J.A.; Carmody, C. Mechanical seal failure analysis. *Tribol. Trans.* **2010**, *53*, 630–635. [CrossRef]
9. Jin, J.; Peng, X.; Jiang, J.; Meng, X.; Zhao, W. Frictional characteristics of impregnated graphite with different graphitization degree versus chromium stainless steel under varying PV values. *Tribol. Int.* **2020**, *146*, 106063. [CrossRef]
10. Jradi, K.; Schmitt, M.; Bistac, S. Surface modifications induced by the friction of graphites against steel. *Appl. Surf. Sci.* **2009**, *255*, 4219–4224. [CrossRef]
11. Zhao, W.; Zhang, G.; Dong, G. Friction and wear behavior of different seal materials under water-lubricated conditions. *Friction* **2021**, *9*, 697–709. [CrossRef]
12. Blau, P.J.; Martin, R.L. Friction and wear of carbon-graphite materials against metal and ceramic counterfaces. *Tribol. Int.* **1994**, *27*, 413–422. [CrossRef]
13. Zhang, N.; Ma, J.; Li, Z.; Zhan, X.; Zheng, Q.; Gao, J.; Liu, Y. Tribological behavior of squamous textured SiC sliding against graphite under mixed lubrication. *J. Manuf. Process.* **2023**, *108*, 639–652. [CrossRef]
14. Zhang, G.; Liu, Y.; Guo, F.; Liu, A.; Wang, Y. Friction characteristics of impregnated and non-impregnated graphite against cemented carbide under water lubrication. *J. Mater. Sci. Technol.* **2017**, *33*, 1203–1209. [CrossRef]
15. Guo, F.; Tian, Y.; Liu, Y.; Wang, Y. Ultralow friction between cemented carbide and graphite in water using three-step ring-on-ring friction test. *Wear* **2016**, *352*, 54–64. [CrossRef]
16. Bernal, J.D. The structure of graphite. *Proc. R. Soc. Lond. Ser. A Contain. Pap. A Math. Phys. Character* **1924**, *106*, 749–773.
17. Bryant, P.J.; Gutshall, P.L.; Taylor, L.H. A study of mechanisms of graphite friction and wear. *Wear* **1964**, *7*, 118–126. [CrossRef]
18. Lancaster, J.K. Transitions in the friction and wear of carbons and graphites sliding against themselves. *ASLE Trans.* **1975**, *18*, 187–201. [CrossRef]
19. Jones, G.A. On the tribological behaviour of mechanical seal face materials in dry line contact: Part I. Mechanical carbon. *Wear* **2004**, *256*, 415–432. [CrossRef]
20. Zhao, H.; Liu, L.; Hu, W.; Shen, B. Friction and wear behavior of Ni–graphite composites prepared by electroforming. *Mater. Des.* **2007**, *28*, 1374–1378. [CrossRef]
21. Rajkumar, K.; Gnanavelbabu, A.; Venkatesan, M.S.; Rajagopalan, K. Cooperating function of graphite in reducing frictional wear of aluminium boron carbide composite. *Mater. Today Proc.* **2018**, *5*, 27801–27809. [CrossRef]
22. Patil, N.; Krishna, P. Friction and wear study of graphite and bronze filled epoxy matrix composites. *Mater. Today Proc.* **2022**, *59*, 134–137. [CrossRef]
23. Zhu, Z.; Bai, S.; Wu, J.; Xu, L.; Li, T.; Ren, Y.; Liu, C. Friction and wear behavior of resin/graphite composite under dry sliding. *J. Mater. Sci. Technol.* **2015**, *31*, 325–330. [CrossRef]
24. He, Z.; Lian, P.; Song, Y.; Liu, Z.; Song, J.; Zhang, J.; Guo, Q. Improving molten fluoride salt and Xe135 barrier property of nuclear graphite by phenolic resin impregnation process. *J. Nucl. Mater.* **2018**, *499*, 79–87. [CrossRef]
25. Goto, H.; Uchijo, K. Wear mechanism of Al–Si alloy impregnated graphite composite under dry sliding. *Wear* **2005**, *259*, 613–619. [CrossRef]
26. Jia, Q.; Yuan, X.; Zhang, G.; Dong, G.; Zhao, W. Dry friction and wear characteristics of impregnated graphite in a corrosive environment. *Chin. J. Mech. Eng.* **2014**, *27*, 965–971. [CrossRef]
27. Zhang, Z.; Qiao, Z.; Wang, X.; Guo, Y.; Wang, D. Comparative study on fretting friction and wear characteristics of different impregnated graphite for sealing application. *Wear* **2024**, *552*, 205455. [CrossRef]
28. Lin, Y.; Liu, T.; Wang, J.; Lu, J.; Dong, X.; Feng, X. Fabrication and oxidation resistance behavior of phosphate/borate impregnation for graphite. *Surf. Coat. Technol.* **2020**, *389*, 125632. [CrossRef]
29. Zhao, J.; Li, Q.; Li, S.; Li, S.; Chen, G.; Liu, X.; Luo, J. Influence of a carbon-based tribofilm induced by the friction temperature on the tribological properties of impregnated graphite sliding against a cemented carbide. *Friction* **2021**, *9*, 686–696. [CrossRef]

30. Zhao, J.; Liu, Y.; Liu, D.; Gu, Y.; Zheng, R.; Ma, R.; Shi, Y. The tribological performance of metal-/resin-impregnated graphite under harsh condition. *Lubricants* **2021**, *10*, 2. [CrossRef]
31. Chen, J.; Gao, S.; Wang, P.; Xue, W.; Li, S.; Duan, D. Study on tribological behavior of zinc phosphate impregnated graphite under oil lubrication condition. *J. Tribol.* **2022**, *144*, 041902. [CrossRef]
32. Zhao, J.; Li, Y.; Liu, Y.; Huang, W.; Xu, Y. Friction and wear performances of impregnated graphite in ring-on-ring tribological test. *Tribol. Int.* **2022**, *174*, 107715. [CrossRef]
33. Coenen, K.T.; Gallucci, F.; Mezari, B.; Hensen, E.J.M.; van Sint Annaland, M. An in-situ IR study on the adsorption of CO_2 and H_2O on hydrotalcites. *J. CO_2 Util.* **2018**, *24*, 228–239. [CrossRef]
34. Sun, Q. The raman OH stretching bands of liquid water. *Vib. Spectrosc.* **2009**, *51*, 213–217. [CrossRef]
35. Huai, W.; Zhang, C.; Wen, S. Graphite-based solid lubricant for high-temperature lubrication. *Friction* **2021**, *9*, 1660–1672. [CrossRef]
36. Larkin, P. *Infrared and Raman Spectroscopy*; Elsevier: Amsterdam, The Netherlands, 2011.

Disclaimer/Publisher's Note: The statements, opinions and data contained in all publications are solely those of the individual author(s) and contributor(s) and not of MDPI and/or the editor(s). MDPI and/or the editor(s) disclaim responsibility for any injury to people or property resulting from any ideas, methods, instructions or products referred to in the content.